# Surface-phonon dispersion of NiAl(110)

M. Wuttig, W. Hoffmann, E. Preuss, R. Franchy, and H. Ibach
*Institut für Grenzflächenforschung und Vakuumphysik, Kernforschungsanlage Jülich, Postfach 1913, D-5170 Jülich 1, Federal Republic of Germany*

Y. Chen, M. L. Xu,* and S. Y. Tong
*Department of Physics and Laboratory for Surface Studies, University of Wisconsin–Milwaukee, Milwaukee, Wisconsin 53201*

(Received 1 May 1990)

We have measured the surface-phonon dispersion for the (110) face of the ordered alloy NiAl using high-resolution electron-energy-loss spectroscopy (EELS) with $\Delta E = 20$–$45$ cm$^{-1}$ both in the [100] ($\bar{\Gamma}$–$\bar{Y}$) and in the [110] ($\bar{\Gamma}$–$\bar{X}$) directions. To identify and fit the observed branches, lattice-dynamical calculations employing a Born–von Kármán model up to third-nearest neighbors were performed. Good agreement between the experimental and calculated dispersion curves is obtained when the force constant between first-layer nickel atoms and second-layer aluminum atoms is increased by 50% and the force constant between first-layer aluminum atoms and second-layer nickel atoms is decreased by 20%. These force-constant changes indicate a surface rippling, where first-layer nickel atoms are displaced inwards and first-layer aluminum atoms are displaced outwards. This is consistent with a structural model based on low-energy electron diffraction (LEED) $I$-$V$ data of Noonan and Davis [Phys. Rev. Lett. **59**, 1714 (1987)] and a medium-energy ion-scattering (MEIS) study by Yalisove and Graham [Surf. Sci. **183**, 556 (1987)].

## I. INTRODUCTION

Properties of alloy surfaces have attracted increasing interest within the last few years. This is, in part, due to progress in materials engineering, which makes it easier to obtain single crystals of alloys in convenient sizes. In part, it is also motivated by the desire to transfer concepts of heterogeneous catalysis obtained for pure metals to bimetallic and more complex systems. Several bimetallic catalysts have already found widespread use in the petrochemical industry,[1] but little is still known about the properties of single-crystal surfaces.

NiAl forms a compositionally ordered alloy with a high heat of formation (58.8 kJ mol$^{-1}$). Its technological importance stems from its hardness, stability, and considerably high melting point (1653 °C). Additionally, NiAl has a large resistance to oxidation, even at elevated temperatures. These properties are rather favorable for an application of NiAl as a high-temperature material, for example, in engines operating at high temperatures.

For our purposes, it is more important that NiAl is one of the few alloy systems which is known to have stable and well-defined surfaces. NiAl has the CsCl crystal structure with a lattice constant of 2.887 Å. The (110) surface consists of Ni and Al atoms within the first layer. Even though these atoms are within one layer, they do not have to be coplanar. This has been shown by low-energy electron-diffraction[2] (LEED) and medium-energy ion-scattering (MEIS) data,[3,4] which show a rippled relaxation of the first layer (see Fig. 1). The aluminum atoms of the first layer are displaced outwards by 4.6% (Ref. 2) or 4.0%,[3] while the nickel atoms of the first layer are displaced inwards by 6.0%.[2,3]

Such a rippled relaxation is certainly not specific for this alloy, but might rather be a common feature of alloy systems with two different constituents in the first layer. Indeed, surface rippling has been observed for a variety

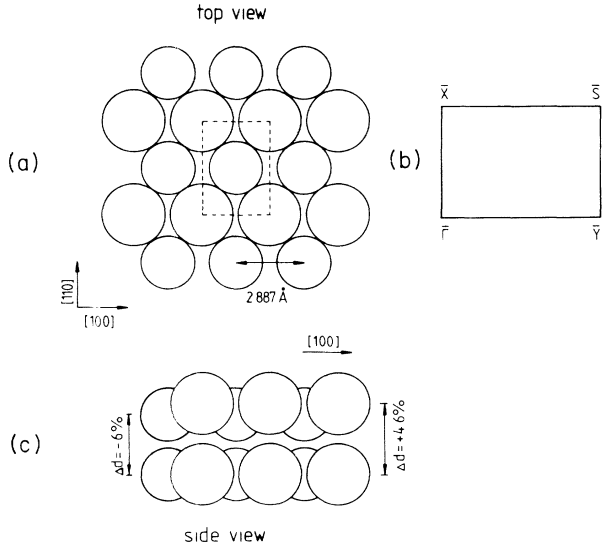


FIG. 1. Structure of the NiAl(110) surface. Top view (top) and side view (bottom) are shown, where the large and small circles denote the aluminum and nickel atoms, respectively. The values for the surface rumpling are from Ref. 2. The Brillouin zone for the (110) surface is shown on the right.

 

of different transition-metal carbides. From the surface-phonon dispersion curves of TiC(100),[5] HfC(100),[6] and ZrC(100),[7] there was strong evidence for surface rippling. This has been confirmed by a LEED analysis[8] for HfC(100). A similar study had already proven that the TaC(100) surface shows a rumpling where first-layer carbon atoms are displaced outwards while first-layer tantalum atoms are displaced inwards.[9]

For NiAl(110) the situation is rather favorable, since the structure determination seems to be quite unique. Both LEED and MEIS give almost identical numbers for the atomic displacements in the first layer. Additionally, the values are in close agreement with a total-energy calculation.[10] This computation shows that the relaxation of atomic orbitals is responsible for the surface rippling.

We have thus chosen the NiAl(110) surface to study surface phonons of a compositionally ordered alloy. This system is also rather interesting from a lattice-dynamical point of view. Surface-phonon dispersion curves have already been measured for a large variety of different elements with fcc and bcc structure.[11] Also, surface-phonon dispersion curves on different faces of compounds with NaCl crystal structure have been investigated.[12,5–7] This is the first time, however, that surface-phonon dispersion curves for a compound with CsCl crystal structure have been measured.

This paper is organized as follows. In Sec. II the experimental details and data are presented. In Sec. III the lattice-dynamical calculations are explained. A discussion is found in Sec. IV.

## II. EXPERIMENT

Sample preparation[13] and a description of the system has been given elsewhere. Here we only want to summarize that the data have been taken at room temperature at a system pressure of $6\times11^{-11}$ mbar. The sample was cleaned by cycles of sputtering and annealing until no more traces of contaminants could be observed either by Auger-electron spectroscopy (AES) or by electron-energy-loss spectroscopy (EELS).

Spectra have been taken both for the $\bar{\Gamma}\,\bar{Y}$ and $\bar{\Gamma}\,\bar{X}$ directions (see Fig. 1). The orientation of the sample in the desired direction was controlled by the position of the (0,1) and (1,0) Bragg peaks, respectively. These peaks were also used to calibrate the momentum-transfer scale. This procedure gives an accuracy of the momentum transfer of 0.02 $\text{Å}^{-1}$. The resolution of the EELS spectrometer was tuned to 30 $\text{cm}^{-1}$ in the $\bar{\Gamma}\,\bar{X}$ direction. In the $\bar{\Gamma}\,\bar{Y}$ direction a resolution of 40 $\text{cm}^{-1}$ was chosen. Since spectra for the $\bar{\Gamma}\,\bar{X}$ direction have been described elsewhere,[13] only spectra for the $\bar{\Gamma}\,\bar{Y}$ direction are presented here.

Before presenting spectra taken for nonvanishing wave-vector transfer (i.e., away from the specular direction), a spectrum is shown in Fig. 2 that is observed in the specular direction. Here the cross section for dipole scattering is very strong, which enabled us to tune the spectrometer to a resolution of 20 $\text{cm}^{-1}$. Figure 2 shows energy-gain and -loss peaks for several surface vibrations at the left- and right-hand sides of the intense elastic peak. Apart from an intense vibration at 220 $\text{cm}^{-1}$ that had already been observed by Lui *et al.*,[14] a resonance is found at 145 $\text{cm}^{-1}$, and two weak features, at 305 and 345 $\text{cm}^{-1}$, are discernible which had not been observed before by Lui *et al.* due to their inferior resolution ($\simeq 50$ $\text{cm}^{-1}$) and a smaller count rate. The dispersion of surface phonons was not measured either, since, typically, the cross section to excite surface phonons away from the specular direction is smaller by at least 2 orders of magnitude.

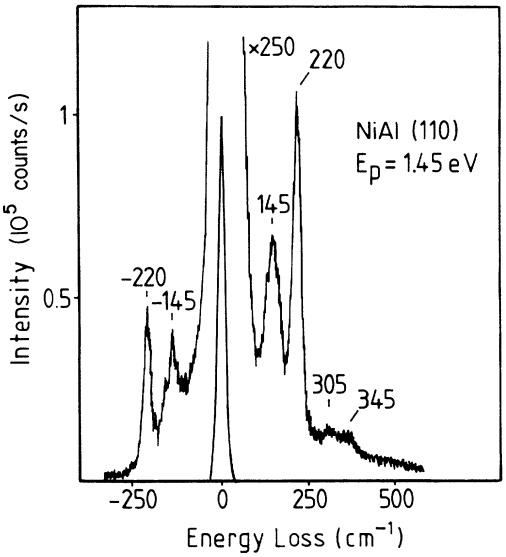


FIG. 2. High-resolution ($\Delta E = 20$ $\text{cm}^{-1}$) spectrum at the $\bar{\Gamma}$ point. Apart from the perpendicular vibration of first-layer aluminum atoms at 220 $\text{cm}^{-1}$, a resonance at 145 $\text{cm}^{-1}$ and two weak features at 305 and 345 $\text{cm}^{-1}$ are observed.

In Figs. 3–5 three different series of spectra are presented, showing the dispersion of different surface phonons in the $\bar{\Gamma}\,\bar{Y}$ direction. In Fig. 3 the dispersion for the energy-loss feature at 220 $\text{cm}^{-1}$ is depicted. This loss is due to the excitation of the perpendicular vibration of first-layer aluminum atoms as already stated by Lui *et al.* This vibration shows almost no dispersion. Over a larger range of the Brillouin zone, there is hardly any shift of the frequency. Additionally, a low-frequency vibration is detected at 60 $\text{cm}^{-1}$ for $\zeta=0.3$ and at 115 $\text{cm}^{-1}$ for $\zeta=0.68$, respectively, where $\zeta$ is the wave vector in reduced units. Three more spectra for this low-frequency vibration are shown in Fig. 4. The frequency of this vibration rises with increasing wave vector from 60 $\text{cm}^{-1}$ (at $\zeta=0.32$) to 143 $\text{cm}^{-1}$ for $\zeta=0.90$. This vibration most likely corresponds to the Rayleigh wave, as discussed in Sec. III.

A similar series of spectra is shown in Fig. 5 for a different primary energy of the impinging electron beam ($E=75$ eV). Some spectra now show even three different energy-gain and -loss peaks. The observation of a second optical mode that has a pronounced dispersion contrary to the perpendicular vibration at 220 $\text{cm}^{-1}$ is important. The corresponding loss peaks shift from 261 $\text{cm}^{-1}$ at $\zeta=0.48$ to 286 $\text{cm}^{-1}$ at $\zeta=0.64$. At the $\bar{\Gamma}$ point this vi-

bration is not observable. The spectra additionally show an almost dispersionless resonance at around 155 $cm^{-1}$ as well as the dispersion of the low-frequency vibration. Above $\zeta=0.6$ these two modes could no longer be resolved for the particular scattering conditions.

It is interesting to note that spectra taken for identical points in the Brillouin zone, but with different primary energy and a different observation angle (spectrum for $\zeta=0.64$ in Figs. 4 and 5) show different modes. This demonstrates the energy and angular dependences of phonon cross sections and will be discussed more explicitly in paper II.[15]

Figure 6 shows the measured dispersion curves for the $\bar{\Gamma}\,\bar{Y}$ and $\bar{\Gamma}\,\bar{X}$ directions. Only the well-resolved energy-gain and -loss peaks have been used to determine the dispersion curves. In the $\bar{\Gamma}\,\bar{Y}$ direction two modes are observed with a large dispersion, while two other modes only have a negligible dispersion. Neither the vibration at 220 $cm^{-1}$ nor the mode at 150 $cm^{-1}$ shows any pronounced dispersion. The acoustic vibration, however, can be followed from 45 $cm^{-1}$ at $\zeta=0.2$ to around 145 $cm^{-1}$ at the $\bar{Y}$ point. The second mode, with a strong dispersion, is not observed at the $\bar{\Gamma}$ point. Its frequency increases from around 250 $cm^{-1}$ at $\zeta=0.45$ to 300 $cm^{-1}$ at $\zeta=1.0$.

In the $\bar{\Gamma}\,\bar{X}$ direction, two acoustic vibrations are observed. The vibration with the higher frequency runs from 110 $cm^{-1}$ at $\zeta=0.45$ to 175 $cm^{-1}$ at $\zeta=1.0$. The second branch shows an almost linear dispersion with increasing wave vector from 30 $cm^{-1}$ at $\zeta=0.3$ to 76 $cm^{-1}$ at $\zeta=1.0$. Additionally, three almost dispersionless vibrations are observed. The branch at around 220 $cm^{-1}$ has already been observed in the $\bar{\Gamma}\,\bar{Y}$ direction. The two other vibrations are found at 300 and 350 $cm^{-1}$, respectively.

The next step in the interpretation of the data is the assignment of the observed branches to certain vibrations and the determination of the corresponding displacement pattern. In principle, the selection rules of inelastic electron scattering[16] and symmetry arguments alone can give much of this information. It was already mentioned that the vibration at 220 $cm^{-1}$ is due to the perpendicular vibration of first-layer aluminum atoms. This vibration is observable at the $\bar{\Gamma}$ point and possesses a large cross section. It, hence, has to be due to a mode that belongs to the total symmetric representation at the $\bar{\Gamma}$ point. At the

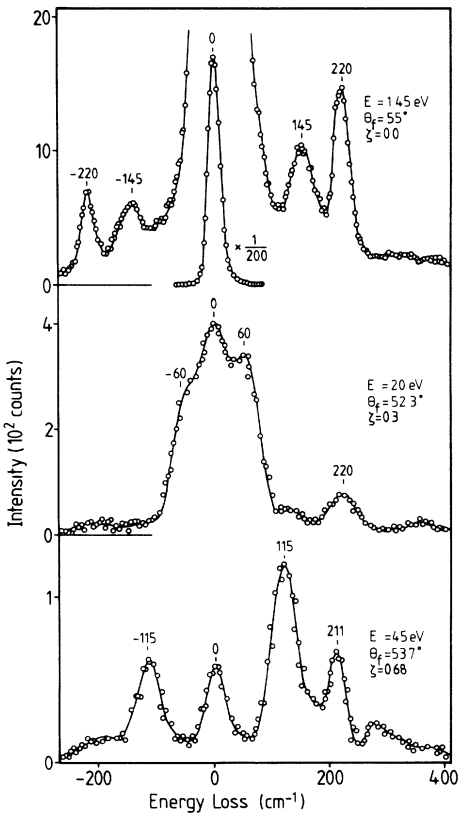


FIG. 3. EELS spectra taken with increasing wave vector in the [100] ($\bar{\Gamma}\,\bar{Y}$) direction. The reduced wave vector is given as well, where $\zeta=1.0$ corresponds to the zone boundary. Additionally, the primary energy and the observation angle for each spectrum are given. This sequence shows the dispersion of the perpendicular aluminum vibration.

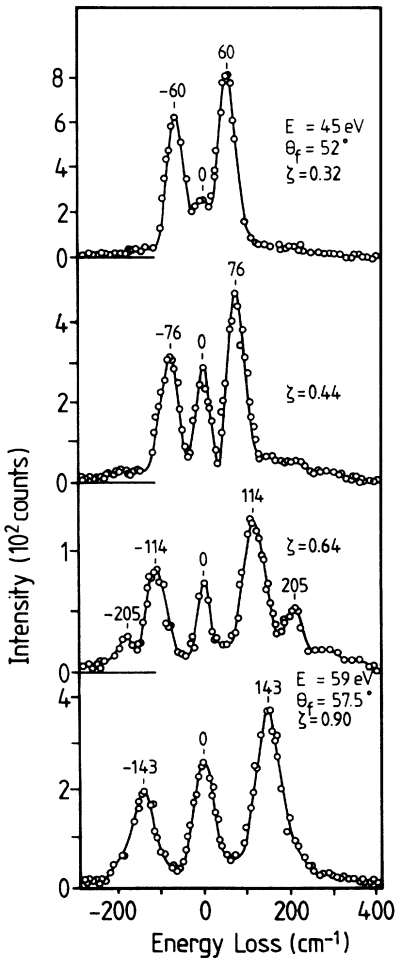


FIG. 4. EELS spectra for the Rayleigh wave.

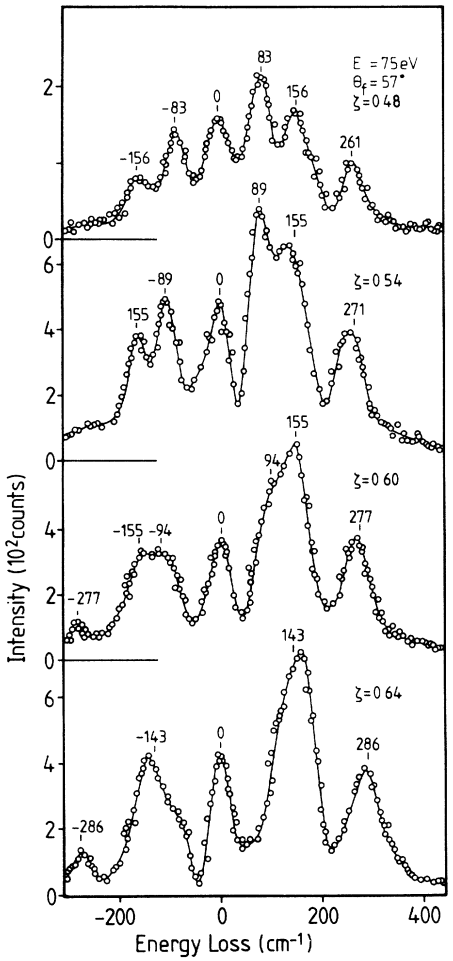


FIG. 5. EELS spectra showing the dispersion of a second optical vibration, together with the surface resonance around 150 $cm^{-1}$ and the Rayleigh wave.

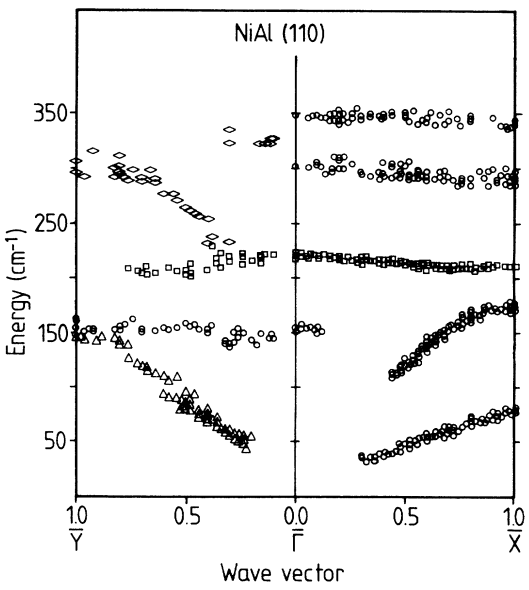


FIG. 6. Experimental data points for the surface-phonon dispersion in the $\bar{\Gamma}\,\bar{Y}$ and $\bar{\Gamma}\,\bar{X}$ directions.

$\bar{\Gamma}$ point, and also at the $\bar{Y}$ and the $\bar{X}$ points, we have a $C_{2v}$ point-group symmetry. All vibrations thus belong to either the $A_1$, $A_2$, $B_1$, or $B_2$ representation. The total symmetric vibrations ($A_i$ representation) have a displacement in the direction of the surface normal only. Since the frequency of 220 $cm^{-1}$ falls into the gap between the optical and acoustic bulk bands, it has to be a localized mode where mainly the light aluminum atoms of the first layer move with phase opposite to the nickel atoms. On the other hand, the second high-frequency mode at 300 $cm^{-1}$ at the $\bar{Y}$ point cannot be a total symmetric vibration at the $\bar{\Gamma}$ point since it is only observed off specular. At the $\bar{\Gamma}$ point all modes belong to either the $A_1$, $B_1$, or $B_2$ vibration, as can be seen from a decomposition of the reducible representation into its irreducible elements. Since in the $\bar{\Gamma}\,\bar{Y}$ direction only $A_1$ and $B_1$ modes—the even modes—can be observed, this vibration has to be of $B_1$ type. Additionally, it also falls into the gap and hence should be a localized aluminum vibration with the polarization strictly parallel to the surface at points $\bar{\Gamma}$ and $\bar{Y}$. These considerations can also be extended to the other observed vibrations. The disadvantage, however, is that group theory does not give precise numbers for the frequencies of certain vibrations, and, thus, cannot be used to determine force constants in the vicinity of the surface. To get this information, lattice-dynamical calculations have to be performed.

## III. LATTICE-DYNAMICAL CALCULATIONS

The first step in any lattice-dynamical calculation consists of a choice of an appropriate model to describe the bulk-phonon dispersion. These bulk vibrations have been measured by Mostoller *et al.*[17] To describe the observed phonons, a Born–von Kármán fit with up to third-nearest neighbors was employed first. With this model the observed bulk-phonon dispersion curves were reproduced quite well. Larger deviations occurred only for the longitudinal-acoustic vibration in the [110] and [111] directions. These modes, however, could be described better if a fourth-nearest-neighbor force-constant model was employed. With this model only minor deviations between the experimental and theoretical curves occur over the entire Brillouin zone.

Owing to the large number of parameters at the surface and to the more complex form of the dynamical matrix, we have considered only interactions up to third-nearest neighbors to calculate the surface-phonon dispersion of NiAl(110). In contrast to Mostoller's work,[17] a central-force-constant model was used. This is no major restriction, since for the interaction up to second-nearest neighbors both central and noncentral models are identical for the CsCl lattice. This statement does not hold for the third-nearest-neighbor interaction, which is characterized by three different values in the noncentral form, but only two different parameters in the central-force-constant model.

Thus, starting from a third-nearest-neighbor central-force-constant model derived from the bulk values used by Mosteller *et al.*,[17] we adjusted various surface force constants to fit *both* the measured dispersion curves and

the inelastic-electron-scattering cross sections at different phonon wave vectors and scattering geometries. The database used in this fitting is enormous. While it is impossible to access the uniqueness of the final force-constant model used, however, the simultaneous fit to dispersion and cross section imposes serious constraints on the final lattice-dynamical model. An interesting result is that the polarization of the lowest two acoustic modes must interchange as the phonon wave vector approaches the zone boundary $\bar{Y}$. This is the *only* way that the measured phonon dispersions and cross sections can be fitted. Details of the fitting procedure and choice of the surface lattice-dynamical model will be the subject of paper II.[15]

In Figs. 7 and 8 we show the results of the lattice-dynamical calculations for a slab of 15 layers using bulk central force constants (up to third-nearest neighbors). The only adjustments to account for the surface environment are (i) to balance the forces on surface atoms so that the net force is zero, and (ii) to impose surface relaxations in the slab according to structural values determined by LEED.[2] The calculated and measured dispersions along lines $\bar{\Gamma}\,\bar{Y}$ and $\bar{\Gamma}\,\bar{X}$ are shown in Figs. 7 and 8, respectively. This bulk-type force-constant model is denoted MB in Table I.

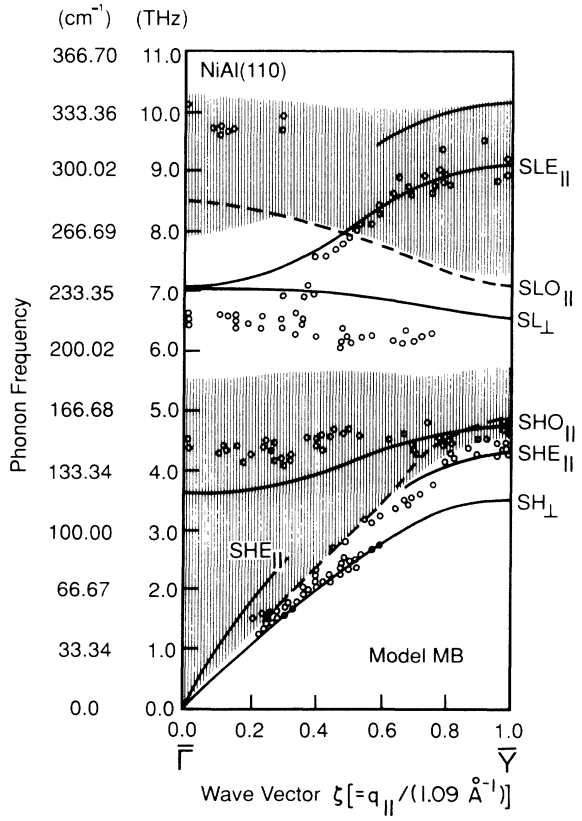


FIG. 7. Calculated phonon dispersion curves for the $\bar{\Gamma}\,\bar{Y}$ direction using the lattice-dynamical model labeled MB in Table I. The solid lines are the dispersion of the even surface modes and resonances, and the dashed lines those of the odd surface modes. The experimental data taken at room temperature are indicated as dots.

Both Figs. 7 and 8 show two bulk-phonon bands separated by a large gap. These bands are due to the broken translational symmetry perpendicular to the surface. Now, modes can be observed at the surface with a given wave vector $\mathbf{q}_{\parallel}$ parallel to the surface, while the momentum transfer $q_z$ perpendicular to the surface can assume an arbitrary value. This produces the quasicontinuum of bulklike modes. For bulk vibrations the atomic displacement at the surface is typically rather small, and they are, hence, hardly observable and play only a minor role in the following discussion. There are some regions in the bulk bands, however, where atomic displacements in the surface region are no longer negligible. Such features appear as so-called surface resonances in the spectra. It will be shown below how these resonances can be identified.

The vibrations in the lower-lying bulk band are modes where mainly the heavier Ni atoms move, while the aluminum atoms hardly participate in the motion. In the upper bulk band, on the other hand, mainly the light aluminum atoms vibrate. The gap between these bulk bands is due to the large mass ratio between nickel and aluminum ($M_{\mathrm{Ni}}/M_{\mathrm{Al}} \simeq 2.2$). Additionally, Figs. 7 and 8 show isolated branches either in the gap between the upper and lower bulk bands, or below the lower bulk bands. These branches describe true surface vibrations with a strong localization. Here, only the very first few layers show a pronounced displacement.

Before we discuss this in more detail, the displacement pattern for the isolated branches is described. Since there

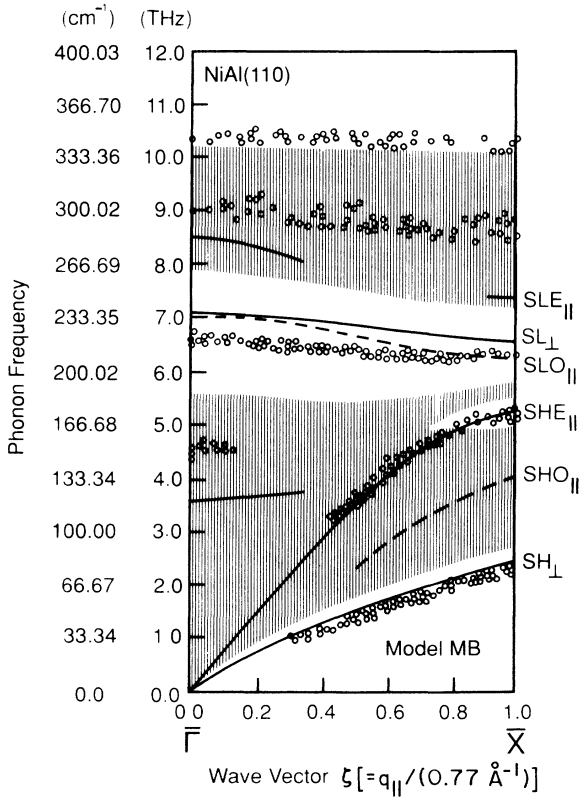


FIG. 8. Same as Fig. 7, but for the $\bar{\Gamma}\,\bar{X}$ direction.

TABLE I. Radial ($\phi''$) and tangential (where $\phi'$ denotes $\phi'/a$, $a=2.887$ Å) force constants for NiAl(110) in a third-nearest-neighbor central-bulk-force model (MB) and an adjusted-surface-force model (MS).

| | Force constants for NiAl(110) (dyn/cm) | | | | |
|---|---|---|---|---|---|
| | MB model | | | MS model | |
| | | | | Bulk- and surface-balanced forces are the same as in the MB model; additional surface-force-constant adjustments | |
| Pair | $r$ (Å) | $\phi''$ | $\phi'$ | | |
| | Bulk | | | | |
| Ni-Al 1NN | 2.50 | 31 420 | 1150 | $\phi''$ (1st layer Al–2nd layer Ni) | 25 136 |
| Al-Al 2NN | 2.89 | 18 380 | 760 | $\phi''$ (1st layer Ni–2nd layer Al) | 47 130 |
| Ni-Ni | | 2 180 | −440 | | |
| Al-Al 3NN | 4.08 | 4 036 | −1484 | $\phi''$ (1st layer Ni–2nd layer Ni) | 3 052 |
| Ni-Ni | | 4 760 | −620 | | |
| | | | | $\phi''$ (1st layer Ni–3rd layer Ni) | 6 664 |
| | Surface (balanced forces) | | | $\phi'_{\text{Ni-Ni}}$ (1st layer, 2NN) | 2 000 |
| $\phi'_{\text{Al-Ni}}$ (1st-2nd layer) | | | 264 | $\phi'_{\text{Ni-Ni}}$ (1st layer, 3NN) | −2 000 |
| $\phi'_{\text{Ni-Ni}}$ (1st-2nd layer) | | | 145 | | |
| $\phi'_{\text{Al-Al}}$ (1st-2nd layer) | | | 724 | | |

is only a $C_s$ point-group symmetry along the [100] and [110] directions, all modes can be classified as being either odd or even with respect to the symmetry plane. The symmetry plane is identical to the scattering plane in our spectrometer configuration. Therefore, selection rules for inelastic electron scattering[16] only allow for the observation of the even modes. At the $\bar{\Gamma}$, $\bar{X}$, and $\bar{Y}$ points, symmetry requirements are stronger, because of the $C_{2v}$ symmetry there. The perpendicular and parallel vibrations in the scattering plane decouple and fall into different irreducible representations.

We now proceed to name the surface phonons. Along $\bar{\Gamma}\,\bar{Y}$ the lowest two branches are nickel-derived surface modes. With use of the bulk-type lattice-dynamical mod-

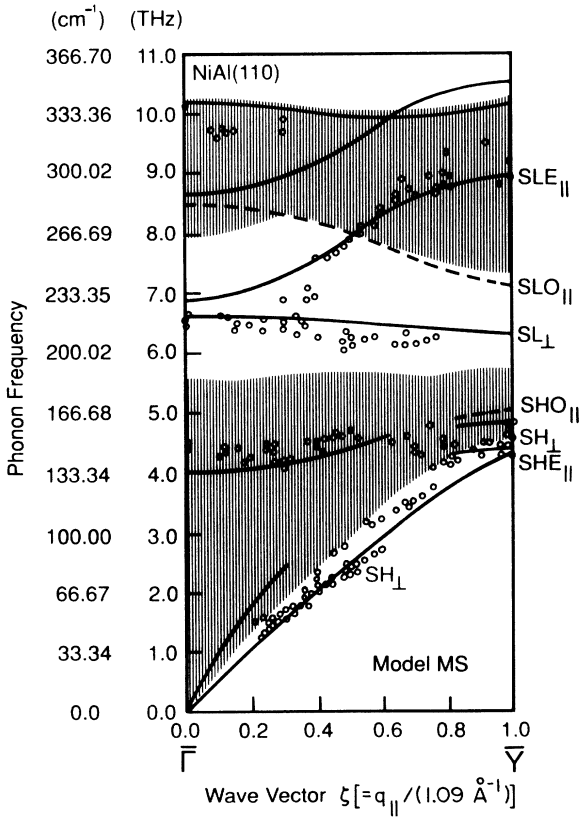


FIG. 9. Same as Fig. 7, but with the surface lattice-dynamical model labeled MS in Table I.

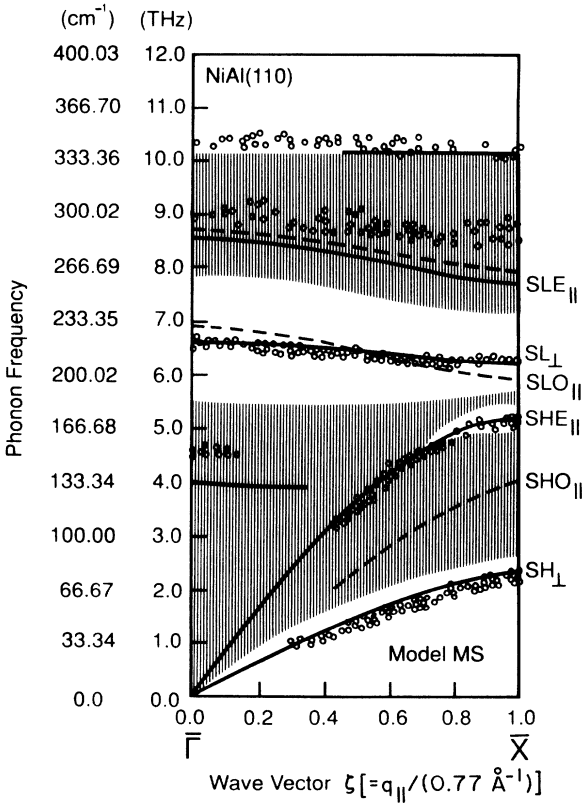


FIG. 10. Same as Fig. 9, but for the $\bar{\Gamma}\,\bar{X}$ direction.

el (i.e., the MB model), the lowest mode at $\bar{Y}$ is (Ni) perpendicularly polarized, and the one above it is (Ni) polarized parallel to the surface and in the scattering plane. We call these two modes $SH_\perp$ and $SHE_\parallel$, respectively (H for the heavier Ni atom). Along $\bar{\Gamma}\bar{X}$, $SH_\perp$ remains the lowest-frequency mode, while $SHE_\parallel$ appears in a gap of the lower bulk band. In the gap between bands, an almost dispersionless mode along $\bar{\Gamma}\bar{Y}$ is perpendicularly polarized (we denote it $SL_\perp$, L for the lighter Al atom), while a $SLE_\parallel$ model disperses up to form a resonance band near midzone. Along $\bar{\Gamma}\bar{X}$, both $SL_\perp$ and $SLO_\parallel$ remain in the gap throughout the zone.

Comparing the experimental data and the calculated dispersion curves using the MB model, it is clear that there are serious discrepancies. In the $\bar{\Gamma}\bar{X}$ direction the calculated frequency of the gap mode $SL_\perp$ is considerably above that of the measured data. The same is true along the $\bar{\Gamma}\bar{Y}$ direction for this mode. Perhaps the most serious discrepancy is at $\bar{Y}$, where the calculated $SH_\perp$ is 1 THz below the data points. Since we expect $SH_\perp$ to have large cross sections (due to the perpendicular displacement of the surface atoms), this mode should be observed. The fact that the data points in the entire region from $0.6\xi$ [$=q_\parallel/(1.09\ \text{Å}^{-1})$] to $\bar{Y}$ are considerably above the calculated frequency dispersion of the $SH_\perp$ mode indicates that the MB model must be wrong. We shall show in paper II that this model gives very poor cross-section comparisons with the data.

We then proceed to adjust the force constants in the near-surface region in order to bring the measured and calculated dispersion curves into better agreement. Noting that we need to lower the calculated frequency of the $SL_\perp$ mode in both directions with respect to the data, we soften the force constant ($\phi''$) between the first-layer Al and second-layer Ni atoms. This softening is consistent with the physical picture of an increased distance between these atoms in a rumpled relaxed surface compared to that of a bulk-terminated structure. We find that a 20% decrease of this force constant leads to a good fit to the data for the $SL_\perp$ mode. The next adjustments are a 50% increase of $\phi''$ between the first-layer Ni and second-layer Al atoms, a 40% increase of $\phi''$ between the first- and second-layer Ni atoms, and a 40% increase of $\phi''$ between the first- and third-layer Ni atoms. These adjustments are also consistent with the physical picture of reduced distances between such atoms in a rumpled surface.

To bring the calculated and measured phonon frequencies and EELS cross section (to be described in paper II) into further agreement, we adjusted the intralayer tangential force constants between Ni atoms in the first layer. Within the first layer, the $\phi'$ between second-nearest-neighbor (NN) Ni atoms is set to 2000 dyn/cm (bulk value $=-440$ dyn/cm), and between third-NN Ni atoms is set to $-2000$ dyn/cm (bulk value $=-620$ dyn/cm). This optimized-surface-force model is labeled MS in Table I.

We now show in Figs. 9 and 10 the calculated phonon dispersion curves using the surface-force model MS, together with the measured data along $\bar{\Gamma}\bar{Y}$ and $\bar{\Gamma}\bar{X}$. The overall quality of the fit is now quite satisfactory. The fit for the $SL_\perp$, $SH_\perp$, and $SHE_\parallel$ modes are all much improved. The most striking feature is that found with use of the MS model, namely that the surface modes $SH_\perp$ and $SHE_\parallel$ are reversed in the order of their frequencies at or near the zone boundary $\bar{Y}$. In other words, the lowest-frequency surface mode now has a (parallel) longitudinal polarization (i.e., $SHE_\parallel$). The surface mode above it now has a perpendicular polarization, i.e., $SH_\perp$. This explains why the measured frequencies shown an apparent upshift as the modes approach the zone edge $\bar{Y}$.

## IV. DISCUSSION

The main force-constant changes used to describe the experimental data were the 50% increase in the force constant between first-layer nickel and second-layer aluminum atoms and the 20% decrease in the force constant between first-layer aluminum and second-layer nickel atoms. In terms of a change of surface structure, the increase of the force constant between first-layer nickel and second-layer aluminum atoms may correspond to an inward relaxation of the nickel atoms. The first-layer aluminum atoms, however, are displaced outwards, since the force constant to second-layer nickel atoms is decreased. This is in qualitative agreement with the observed surface rumpling. It is also interesting to note how sensitive the surface force constants are on the surface relaxations. A 6% inward relaxation corresponds to a 50% increase of the corresponding force constant. Because of the complexity of the surface charge redistribution, one cannot determine surface structure quantitatively based only on the force-constant changes. A study of the surface structure for NiAl(110) using EELS cross-section analysis will be presented in the following paper.[15]

While the surface-adjusted force-constant model (MS) may not be unique, we have shown in this paper that it produces rather satisfactory fits to the measured dispersion curves. More severe constraints are imposed on the surface lattice-dynamical model in the following paper,[15] where we compare the calculated inelastic cross-section spectra to data for different $\mathbf{q}_\parallel$ values, incident energies, and scattering geometries.[16,18–20] We shall show that the model labeled as MS in Table I works very well.

## ACKNOWLEDGMENTS

This work was supported by the U.S. Department of Energy, under Grant No. DE-FG02-84ER45147, and by Petroleum Research Fund Grant No. 1154-AC5,6 administered by the American Chemical Society.

*Present address: Department of Chemistry, University of Toronto, Lash Miller Chemical Laboratories, Toronto, Canada M5S 1A1.

[1]J. H. Sinfelt, Sci. Am. **253**(3), 96 (1985).

[2]J. R. Noonan and H. L. Davis, Phys. Rev. Lett. **59**, 1714 (1987).

[3]S. M. Yalisove and W. R. Graham, Surf. Sci. **183**, 556 (1987).

[4]D. Mullins and S. Overbury, Surf. Sci. **199**, 141 (1988).

[5]C. Oshima, M. Wuttig, T. Aizawa, R. Souda, S. Otani, Y. Ishizawa, H. Ishida, and T. Terakura, Phys. Rev. B **36**, 7510 (1987).

[6]M. Wuttig, C. Oshima, T. Aizawa, R. Souda, S. Otani, and Y. Ishizawa, Surf. Sci. **192**, 573 (1987).

[7]R. Franchy, C. Oshima, T. Aizawa, R. Souda, S. Otani, and Y. Ishizawa, J. Electron Spectrosc. **44**, 317 (1987).

[8]G. R. Gruzalski, D. M. Zehner, J. R. Noonan, H. L. Davis, R. A. DiDio, and K. Müller, J. Vac. Sci. Technol. A **7**, 2054 (1989).

[9]J. R. Noonan, H. L. Davis, and G. Gruzalski, J. Vac. Sci. Technol. A **5**, 787 (1987).

[10]M. H. Kang and E. J. Mele, Phys. Rev. B **36**, 7371 (1987).

[11]See, e.g., J. P. Toennies, in *Proceedings of the Solvay Conference on Surface Science,* edited by F. W. deWette (Springer, Heidelberg, 1988), p. 248.

[12]G. Brusdeylins, R. B. Doak, and J. P. Toennies, Phys. Rev. B **27**, 3662 (1983).

[13]M. Wuttig, W. Hoffmann, E. Preuss, R. Franchy, and H. Ibach, Vacuum (to be published).

[14]S. C. Lui, J. Mundenar, E. W. Plummer, M. Mostoller, R. M. Nicklow, D. M. Zehner, W. K. Ford, and J. Erskine, in *Physical and Chemical Properties of Thin Metal Overlayers and Alloy Surfaces,* Mater. Res. Soc. Symp. Proc. No. 83, edited by D. M. Zehner and D. W. Goodman (MRS, Pittsburgh, 1987), p. 59.

[15]Y. Chen, M. L. Xu, S. Y. Tong, M. Wuttig, W. Hoffmann, R. Franchy, and H. Ibach, this issue, the following paper, Phys. Rev. B **42**, 5451 (1990).

[16]S. Y. Tong, C. H. Li, and D. L. Mills, Phys. Rev. Lett. **59**, 1714 (1980); H. Ibach and D. L. Mills, *Electron Energy Loss Spectroscopy and Surface Vibrations* (Academic, New York, 1982).

[17]M. Mostoller, R. Nicklow, D. M. Zehner, S. C. Lui, J. M. Mundenaar, and E. W. Plummer, Phys. Rev. B **40**, 2856 (1989).

[18]M. L. Xu, B. M. Hall, S. Y. Tong, M. Rocca, H. Ibach, S. Lehwald, and J. E. Black, Phys. Rev. Lett. **54**, 1171 (1985).

[19]Z. Q. Wu, Y. Chen, M. L. Xu, S. Y. Tong, S. Lehwald, M. Rocca, and H. Ibach, Phys. Rev. B **39**, 3116 (1989).

[20]S. Y. Tong, C. H. Li, and D. L. Mills, Phys. Rev. B **24**, 806 (1981).